Bulletin of the Seismological Society of America, Vol. 93, No. 4, pp. 1433–1448, August 2003

Secondary Aftershocks and Their Importance for Aftershock Forecasting

by Karen R. Felzer, Rachel E. Abercrombie, and Göran Ekström

Abstract The potential locations of aftershocks, which can be large and damaging, are often forecast by calculating where the mainshock increased stress. We find, however, that the mainshock-induced stress field is often rapidly altered by aftershock-induced stresses. We find that the percentage of aftershocks that are secondary aftershocks, or aftershocks triggered by previous aftershocks, increases with time after the mainshock. If we only consider aftershock sequences in which all aftershocks are smaller than the mainshock, the percentage of aftershocks that are secondary also increases with mainshock magnitude. Using the California earthquake catalog and Monte Carlo trials we estimate that on average more than 50% of aftershocks produced 8 or more days after $M \geq 5$ mainshocks, and more than 50% of all aftershocks produced by $M \geq 7$ mainshocks that have aftershock sequences lasting at least 15 days, are triggered by previous aftershocks. These results suggest that previous aftershock times and locations may be important predictors for new aftershocks. We find that for four large aftershock sequences in California, an updated forecast method using previous aftershock data (and neglecting mainshock-induced stress changes) can outperform forecasts made by calculating the static Coulomb stress change induced solely by the mainshock.

Introduction

It has long been observed that aftershocks may produce their own aftershocks, commonly known as secondary aftershocks (Richter, 1958). The essential definition of secondary aftershocks is that they are primarily or entirely triggered by a previous aftershock and show pronounced spatial and temporal clustering around this aftershock. The fraction of aftershocks that are secondary is often assumed to be small. There is good reason to question this assumption, however, with important implications for aftershock forecasting. If secondary aftershock production is indeed low, then the best way to forecast aftershock locations should be by calculating the stress changes produced by the mainshock (e.g., Rybicki, 1973; Das and Scholz, 1981; Harris and Simpson, 1992; King *et al.*, 1994; Stein *et al.*, 1997; Taylor *et al.*, 1998; Zeng, 2001; Kilb, 2003). If secondary aftershocks are common, however, many aftershocks might not be predictable without using the locations and times of previous aftershocks. Indeed, for general seismicity, many authors have successfully used the locations of previous earthquakes to predict the distribution of future ones (e.g., Kagan and Jackson, 1991; Cao *et al.*, 1996; Woo, 1996; Jackson and Kagan, 1999; Kafka and Levin, 2000; Kagan and Jackson, 2000; Wiemer, 2000; Kafka, 2002).

In this article we use statistical tests to demonstrate that secondary aftershocks are a common phenomenon and then use Monte Carlo modeling to quantify how many aftershocks are secondary in the average California aftershock sequence. We also show that while the exact factors that determine aftershock location may be many and complex, using only the locations and times of previous aftershocks can produce a more precise forecast of aftershock locations than using the calculations of the static Coulomb stress changes induced solely by the mainshock.

Evidence for Secondary Aftershocks

The Aftershock Production Rate of Small Earthquakes

Most aftershocks are small. Therefore secondary aftershocks may be common only if small earthquakes, as a group, are capable of producing a substantial number of aftershocks. It has been recognized that the volumetric static stress change produced by small aftershocks (when integrated over a finite volume) is essentially negligible in comparison to that produced by the mainshock (e.g., Hardebeck, 1998). The relative ability of two earthquakes to induce volumetric static stress change is not, however, equal to their relative ability to produce aftershocks. The Gutenberg–Richter relationship states that the total number of earthquakes in a population that are larger than or equal to some magnitude M varies as 10^{-bM} (Ishimoto and Iida, 1939; Gutenberg and Richter, 1944). Volumetric static stress change varies with earthquake moment, which varies with earthquake magnitude, M, as $10^{1.5M}$ (Kanamori, 1977). In contrast, aftershock productivity varies much more slowly

with mainshock magnitude, as 10^{bM} (Reasenberg and Jones, 1989; Yamanaka and Shimazaki, 1990; Kagan, 1991; Felzer *et al.*, 2002), where b is the parameter from the Gutenberg–Richter relationship for the aftershock population, and is typically found to be close to 1. The physical reason why aftershock production varies as 10^{bM} rather than with volumetric static stress change is not presently known, although we note that other seismic properties that vary as 10^{M} are dynamic displacement, velocity, and acceleration in the far field (Richter, 1958) and mainshock faulting area, if we assume a constant stress drop (Kanamori and Anderson, 1975).

To solve for the relative aftershock productivity of small and large earthquakes we need to multiply the expression giving the number of aftershocks as a function of mainshock magnitude by the number of potential mainshocks in each magnitude range. The latter is given by the Gutenberg–Richter relationship. We assume that the b-value for aftershocks is the same as the b-value for the general population (Ranalli, 1969). We note that the assumption of identical b-values is additionally supported by the mathematical demonstration of Woo (1996) that subpopulations of earthquakes cannot have different b-values if the population as a whole adheres to the Gutenberg–Richter relationship. Assuming equal b-values, the product of the aftershock production relationship and Gutenberg–Richter relationship is given by $10^{-bM} \times 10^{bM} =$ a constant. That is, the total number of aftershocks produced by each magnitude range is the same, regardless of the magnitude range being considered (Michael and Jones, 1998; Felzer *et al.*, 2002). Thus the total number of aftershocks produced by small earthquakes, and hence the total number of secondary aftershocks produced by small aftershocks, is expected to be significant.

Secondary Aftershocks and Omori's Law

Utsu (1962) and Page (1968) have argued that few aftershocks are secondary because most aftershock sequences decay smoothly with time after the mainshock in accordance with the modified Omori law (Utsu, 1961). This law is given by

$$R = A(t + c)^{-p}, \tag{1}$$

where R is the aftershock rate, t is time after the mainshock, and A, p, and c are constants. It is usually found that p is slightly larger than 1 and c is on the order of a fraction of a day (e.g., Reasenberg and Jones, 1989). The smooth adherence of most aftershock sequences to the modified Omori law is taken by Utsu (1962) and Page (1968) to indicate a paucity of secondary aftershocks because secondary aftershocks should cluster close in time to the aftershock that triggered them, creating sharp peaks in the aftershock decay time series. Utsu (1962) and Page (1968) were correct that such temporal peaks should occur, but they erred in their implicit assumption that the peaks should rise higher than the average noise level. In fact, if secondary aftershocks are continuously being triggered by small aftershocks, then most of them should occur in small sequences that constitute small and frequent temporal peaks that blend into one another.

That it is possible for an aftershock sequence adhering well overall to Omori's law to in fact be made up of many different overlapping aftershock sequences, each individually adhering to Omori's law, has been demonstrated theoretically (Sornette and Sornette, 1999; Helmstetter and Sornette, 2002). In order to test these results for individual aftershock sequences we generate synthetic sequences using the statistical aftershock production model of Felzer *et al.* (2002). In this model earthquakes are generated to either follow a modified Omori decay rate initiating at the time of the mainshock (direct aftershocks) or initiating at the time of a previous aftershock (secondary aftershocks). The other rules of the model are that aftershock magnitudes are selected randomly from the Gutenberg–Richter distribution, aftershock productivity varies as 10^{bM}, and aftershocks produce aftershocks at the same rate that other earthquakes do (for rationalization of the assumptions, see Felzer *et al.* [2002]).

This general method for the statistical generation of synthetic aftershocks is similar to that used by Ogata (1988), Kagan (1991), Console and Murru (2001), and Helmstetter and Sornette (2002). Models of this type have been found to produce synthetic aftershock sequences that are in excellent agreement with real aftershock time series (Ogata, 1988; Guo and Ogata, 1997; Felzer *et al.*, 2002). We generate a trial sequence with this model, using a mainshock of M 7 and the average California modified Omori parameters (see the Variation of Secondary Aftershocks with Time section). Forty-seven percent of the aftershocks in our trial synthetic sequence are secondary. Yet the time series of the sequence shows no excursion beyond the 95% confidence intervals for Poissonian variation around the modified Omori law (Fig. 1). Thus by counterexample we have proven that the absence of significant deviation from the modified Omori law does not imply a rarity of secondary aftershocks.

Testing for the Existence of Secondary Aftershocks

We propose that a better test for the existence of secondary aftershocks is to search for temporal correlations between aftershocks on a local scale. We test this idea on a sample of nine large California aftershock sequences (Fig. 2). The epicentral information for the mainshocks and the spatial limits used for the aftershock zones, which are rectangles selected by visual inspection, are given in Table 1. The data are taken from the Council of the National Seismic System catalog. All of the mainshocks are $M > 6$, except for the Oceanside and Palm Springs earthquakes (M 5.4 and M 5.6, respectively), which we observe had unusually large aftershock sequences for their magnitudes. The half-widths of the aftershock zones are between one and two times the fault length of the mainshock. We use all $M \geq 2$ aftershocks that occurred from the time of the mainshock through December 2001, with the exception of the Joshua Tree aftershock sequence, which we use only until the time of the

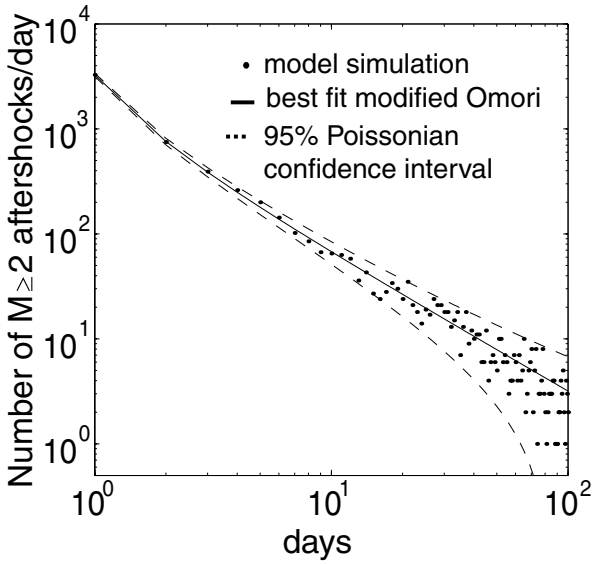

Figure 1. Time series of a simulated aftershock sequence of an M 7 California mainshock (dots) (using average California parameters; see Table 3), fit with the modified Omori law (solid line) and plotted with the 95% confidence intervals for expected Poissonian random fluctuation (dashed lines). Although none of the data points lie outside of the 95% confidence intervals, 47% of the aftershocks are secondary. We conclude from this counterexample that the absence of significant deviation from the modified Omori law need not indicate that few aftershocks are secondary. Note that each data point represents the total number of aftershocks to occur on the day in question, rather than the instantaneous aftershock rate at a particular time (for example, the first data point gives the total of all aftershocks that occurred in the first 24 hr of the sequence.) This accounting system in combination with the small c parameter value of the total aftershock sequence ($c \approx 0.05$) causes the graph to curve upward at small times on the log–log plot. For aftershock sequences in which c is larger than about 0.2, or aftershock recording on the first day is incomplete, upward concavity on plots of this type should be negligible.

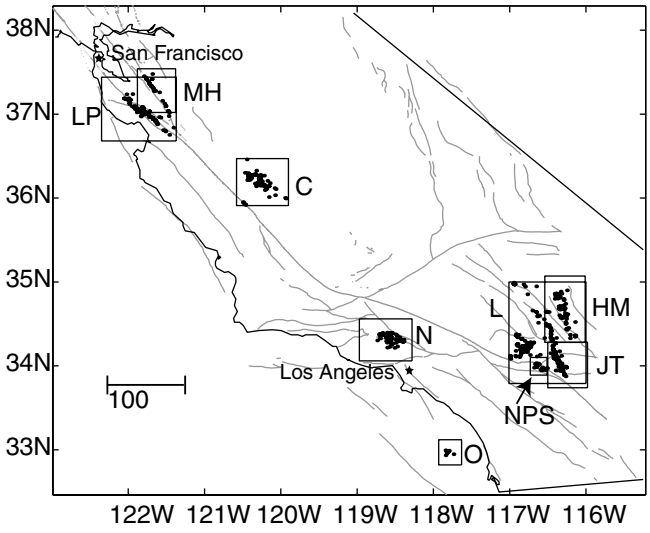

Figure 2. California aftershock sequences used in this study. The aftershock zone boundaries were determined using all aftershocks recorded in each sequence, but only $M \geq 4$ aftershocks are plotted on the figure. The mainshocks are C, Coalinga; MH, Morgan Hill; NPS, North Palm Springs; O, Oceanside; LP, Loma Prieta; JT, Joshua Tree; L, Landers; N, Northridge; and HM, Hector Mine. The cities of Los Angeles and San Francisco are also labeled for reference.

Landers mainshock, and the Landers aftershock sequence, which we use only through the time of the Hector Mine mainshock. We draw "influence zone" boxes around each aftershock epicenter with the half-widths of the influence zones equal to two times the estimated fault length. The influence zones are not expected to contain all of the secondary aftershocks of a given aftershock, since there is presently no known physical limit on how far away a secondary aftershock can be. Nor are the earthquakes in a given influence zone expected to be exclusively secondary aftershocks of the target aftershock, as secondary aftershock zones undoubtedly intersect and direct aftershocks may be scattered throughout. The influence zones are chosen to encompass an area that is large enough such that we expect to capture many secondary aftershocks if they exist, while at the same time small enough such that any signal of secondary aftershock temporal clustering can be seen. To draw the influence zones, mainshock fault length is estimated from the equations of Kanamori and Anderson (1975), assuming a circular fault and a constant stress drop of 30 bars, and using the earthquake moment that is calculated from $M_0 = 10^{1.5M+10.73}$ (Kanamori, 1977). The resulting fault length is similar to that estimated empirically by Wells and Coppersmith (1994). We draw the boxes for the influence zones in map view and do not use depth in our calculation. This is done for simplicity and because depths are more poorly constrained than epicenters.

To test for the presence of temporal clustering within the influence zones we measure the percentage of all aftershocks that occur less than 24 hr after and within the influence zone of a previous aftershock. We call this percentage the spatiotemporal correlation index. To test whether the value of the spatiotemporal correlation index indicates actual interaction between aftershocks rather than just coincidental correlation, we remeasure the index after shuffling the aftershock times and locations. In this process all of the aftershock times and locations are preserved, but they are randomly recombined with one another. We then test the null hypothesis that the real and recombined catalogs come from a base population with the same spatiotemporal correlation index (i.e., there is no real correlation between the aftershocks). If multiple data samples are taken from a single large population, the differences between the percentages of events in each sample satisfying a given criterion should be normally distributed. We thus compute z statistics to deter-

Table 1
Epicentral Information and the Aftershock Zones Used for Mainshocks in This Study

Earthquake	Date (mm/dd/yy)	Magnitude	Epicenter	Aftershock Zone, N–S	Aftershock Zone, E–W
Coalinga	05/02/83	6.7	36.23, −120.32	35.91/36.47	−120.58/−119.90
Morgan Hill	04/24/84	6.2	37.31, −121.68	37.02/37.54	−121.88/−121.38
N. Palm Springs	07/08/86	5.6	34.0, −116.61	33.89/34.1	−116.73/−116.51
Oceanside	07/13/86	5.4	32.97, −117.87	32.82/33.12	−117.93/−117.63
Loma Prieta	10/18/89	7.0	37.04, −121.88	36.68/37.44	−122.35/−121.37
Joshua Tree	04/23/92	6.1	33.96, −116.32	33.74/34.28	−116.50/−115.98
Landers	06/28/92	7.3	34.20, −116.44	33.79/35.00	−117.01/−116.00
Northridge	01/17/94	6.7	34.21, −118.54	34.06/34.56	−118.97/−118.28
Hector Mine	10/16/99	7.1	34.59, −116.27	34.28/35.07	−116.45/−116.01

mine whether the real and recombined catalogs might come from the same statistical population (null hypothesis). Using this procedure we find that for every sequence the null hypothesis can be rejected at a confidence level of over 99.99%, with the higher spatiotemporal correlation occurring in the real catalog. This indicates that there is real temporal-spatial clustering between the aftershocks. Therefore, in the absence of any plausible alternative explanation for the correlation, we can infer that secondary aftershocks are present in all of the aftershock sequences.

Secondary Aftershock Rates in the Average California Aftershock Sequence

In the previous section we demonstrated with high likelihood that secondary aftershocks are routinely and significantly present in aftershock sequences, but we have not quantified how many there are. The synthetic aftershock generation model described earlier can be used to solve for the percentage of aftershocks that are secondary after particular mainshock magnitudes and elapsed times. It is also possible to write several equations such that the number of aftershocks that are secondary can be easily estimated for any time and mainshock magnitude. In this section we will derive these equations and the parameters necessary to solve them.

Variation of Secondary Aftershocks with Time

Both direct and total aftershock sequences follow the modified Omori law, where the total aftershock sequence is the sum of the direct and secondary sequences. Therefore, the general equation for the fraction, $S_0(t)$, of ongoing aftershocks at time t that are secondary is given by

$$S_0(t) = 1 - \frac{A_D(t + c_D)^{-p_D}}{A_T(t + c_T)^{-p_T}}, \quad (2)$$

where A_D, c_d, p_D, A_T, c_T, and p_T are the modified Omori parameters for the direct and total aftershock sequences, respectively.

To solve for the fraction of cumulative aftershocks occuring from the time of the mainshock until some end time, t, that are secondary, we first calculate the cumulative number of direct aftershocks, C_D, and total aftershocks, C_T, by integrating the modified Omori law (equation 1) over time from 0 to t:

$$C_D = \frac{A_D}{1 - p_D}\left((t + c_D)^{1-p_D} - c_D^{1-p_D}\right) \quad (3a)$$

and

$$C_T = \frac{A_T}{1 - p_T}\left((t + c_T)^{1-p_T} - c_T^{1-p_T}\right), \quad p_D \neq 1,\ p_T \neq 1. \quad (3b)$$

The fraction of cumulative aftershocks that are secondary, $S_c(t)$, is then given by

$$S_c(t) = 1 - C_D/C_T. \quad (4)$$

To find the average parameters for these equations for California, we count the cumulative number of $M \geq 4.8$ aftershocks that occurred at intervals from 0.02 to 180 days after $M \geq 5.0$ California mainshocks. The cutoff of M 4.8 is used because we determine using the Gutenberg–Richter relationship that this is the smallest magnitude to which all of the data are complete (in particular there is potentially very low reporting of small aftershocks immediately after $M > 7$ mainshocks in the data set [K. Hutton, personal comm., 1999]). Using a cutoff below the completeness magnitude would reduce the statistical accuracy of the results. We use all mainshocks that occurred between 1975 and 2000, except for mainshocks in the Mammoth Lakes volcanic area, because volcanic and tectonic earthquakes may be governed by different processes and have different parameters. We also omit (1) mainshocks that occurred as such early aftershocks of previous earthquakes that their own aftershocks could not be reliably determined and (2) mainshocks that had aftershocks larger than themselves before 180 days had elapsed. This leaves a total of 73 $M \geq 5$ earthquakes. We

determine the aftershock region of each earthquake by visually selecting the area with highly clustered earthquakes after the mainshock. In the vast majority of cases, the half-lengths of these regions are between one and two times the fault length of the mainshock. After defining the regions we find a total of 80 recorded $M \geq 4.8$ aftershocks, for all of the mainshocks, over 180 days.

Since some of the individual aftershock sequences contain few earthquakes we stack the aftershock data to form a single average sequence, from which we solve for the modified Omori parameters. In stacking the data we follow the premise of Dieterich (1994) and assume that aftershock sequences triggered by mainshocks of different magnitudes have the same duration. In order to normalize the parameters from the stacked sequence we first divide the number of aftershocks in the stack by the total number of mainshocks and then determine the magnitude of the equivalent mainshock that would produce a sequence of this size. Finding the magnitude of the equivalent mainshock is done using the magnitudes of the mainshocks of the individual sequences. First we note that since aftershock production varies with mainshock magnitude as 10^{bM}, and since the aftershocks follow the Gutenberg–Richter relationship, we expect that at any given time the accumulated number of aftershocks should be equal to $10^{b(M-C(t)-m_c)}$, where $C(t)$ is a value that decreases with time and m_c is the smallest magnitude aftershock counted. We find that an appropriate b-value for California is 1.0 ± 0.01, using a least-squares algorithm in which each data point is weighted by the number of earthquakes it represents (Bender, 1983). To solve for this b-value we use a magnitude completeness cutoff of M 2.6 for southern California and M 2.2 for northern California and eliminate data in the Mammoth Lakes region and north of the triple junction, both places where we find the completeness magnitudes to be larger than M 3. We solve for the cutoff magnitudes by using a χ^2 test to find the lowest magnitude for which the Gutenberg–Richter function still adequately describes the data at the 95% confidence level. For comparison, other authors have found b-values of 0.99 (Wiemer and Wyss, 2002) and 1.0 (Stein and Hanks, 1998) for southern California. Using a b-value of 1.0 we then combine all of the mainshock magnitudes to solve for the equivalent mainshock magnitude, m_e,

$$
\begin{aligned}
10^{m_e - C - 4.8} &= (1/73) \sum_{i=1}^{i=73} 10^{m(i) - C - 4.8} \\
10^{m_e} &= (1/73) \sum_{i=1}^{i=73} 10^{m(i)} \qquad (5) \\
m_e &= 6.04 \ ,
\end{aligned}
$$

where the $m(i)$s are the magnitudes of the individual mainshocks. This means that we expect the average M 6.04 California mainshock to produce the average number of $M \geq 4.8$ aftershocks in our stack, which is 80 aftershocks/73 mainshocks = 1.2 aftershocks, over 180 days. The parameters that we solve for from the average sequence should then give us the fraction of aftershocks that are secondary in the average aftershock sequence that follows an M 6.04 mainshock and contains no aftershocks larger than the mainshock.

Solving for the Direct Sequence Omori's Law Parameters. We solve for the direct Omori parameters A_D, c_D, and p_D for the average California aftershock sequence by using the statistical aftershock-generating model described earlier to perform a grid search. In this process, a range of parameter values are tested (0.087–0.11 for A_D, 0.01–0.15 for c_D, and 1.05–1.4 for p_D), then the averaged results of multiple model runs are compared with the data. We search for the set of parameters that minimizes the least-squares error between the synthetic sequences and the data. A set b-value of 1.0 is also used as input to the aftershock-generating model. The model also requires one more parameter, M_{min}, the magnitude of the smallest existing earthquake. We chose to set $M_{min} = 0$ based on the results of Abercrombie (1995), that earthquakes at least as small as M 0 have stress drops comparable to those of other earthquakes, and on the results of Richardson and Jordan (2002), that M 0 may be the minimum magnitude for traditional shear-failure earthquakes. If the true M_{min} is less than 0, then more aftershocks are secondary than the parameters we solve for would predict; conversely, if $M_{min} > 0$, fewer aftershocks are secondary. The effect of a particular change in M_{min} depends on the magnitude of the mainshock (if we only consider aftershocks smaller than the mainshock) and is proportional to $(M_{min} - \Delta M_{min})/(M - M_{min})$, where M is the magnitude of the mainshock. That is, since each magnitude range produces an equal number of aftershocks, the change in secondary aftershocks due to a change in M_{min} is proportional to the fractional change of magnitude ranges.

Our resulting best-fit direct sequence parameters for California are $A_D = 0.0921$ days^{p-1}, $p_D = 1.37$, and $c_D = 0.085$ days (Table 3). This value of A_D specifically gives the number of $M \geq 4.8$ aftershocks produced by an M 6.04 mainshock. The value may be adjusted for some other aftershock magnitude cutoff m_c by multiplying it by $10^{4.8 - m_c}$ and adjusted to describe an aftershock sequence initiated by another mainshock with magnitude M by multiplying it by $10^{M - 6.04}$.

Solving for the Total Sequence Omori's Law Parameters. We use a nonlinear least-squares fit to solve for the total sequence modified Omori law parameters directly from our average California aftershock sequence data. Sornette and Sornette (1999) demonstrated that stacking direct and secondary aftershock sequences actually causes the total aftershock sequence to have modified Omori law parameters that vary with time. Specifically, if p_D is equal to $1.0 + \theta$, then p_T should vary smoothly with time from $1.0 - \theta$ to $1.0 + \theta$, where θ is a value between 0 and 1. A_T should also increase with time. This temporal parameter variation is the

Table 2
Comparison of Probability Map and Coulomb Stress Change Predictions of $M \geq 5$ Aftershocks

Mainshock	Aftershock Date (mm/dd/yy)	Aftershock Magnitude	Real-time Prob. Map	24-hr Prob. Map	Coulomb Map
Joshua Tree	05/18/92	5.0	5	6	2
Joshua Tree	06/28/92	7.3	1	378	108
Landers	06/28/92	5.1	576	NA	213
Landers	06/28/92	5.0	576	NA	229
Landers	06/29/92	5.0	19	NA	57
Landers	06/29/92	5.5	6	NA	66
Landers	07/01/92	5.3	89	15	18
Landers	07/05/92	5.4	2090	2090	1337
Landers	07/24/92	5.0	107	23	393
Landers	08/17/92	5.0	78	88	182
Landers	09/15/92	5.1	50	290	103
Landers	11/27/92	5.4	1	217	471
Landers	12/04/92	5.2	5	301	840
Landers	08/21/93	5.0	72	102	138
Landers	06/16/94	5.0	161	141	1965
Landers	03/18/97	5.1	1	288	413
Landers	10/16/99	7.1	1	291	1262
Hector Mine	10/21/99	5.0	241	27	72
Hector Mine	10/21/99	5.0	230	21	92
Hector Mine	10/22/99	5.0	3	265	92

The first three columns give the mainshock and the date and magnitude of the aftershock. The next three columns give the ranking of the cell that the aftershock occurred in on the real-time probability map, the 24-hr probability map, and the Coulomb static stress change map, respectively. A number 1 ranking indicates that the cell was predicted to be the most likely one to contain an aftershock. "NA" indicates that the aftershock occurred too early to be eligible for a 24-hr probability map prediction.

likely explanation for the observations of Mogi (1962) and Gross and Kisslinger (1994) that the later parts of many aftershock sequences are not well fit with the same parameters that describe the initial activity. For simplicity, however, we first solve for a single set of Omori parameters that best fits the entire sequence (Table 3; Fig. 3). Our best-fit p_T parameter is 1.08, the same average p_T that was found by Reasenberg and Jones (1989) in a study of 62 California aftershock sequences. Our best-fit A_T parameter is lower than that found

Table 3
Average Modified Omori Law Parameters for California Aftershock Sequences

Parameter Type	Days	A, days^{1-p}	p	c, days
Direct sequence	All	0.0921	1.37	0.085
Total sequence	All	0.116	1.08	0.014
Total sequence	0–1	0.151	0.75	10^{-5}
Total sequence	2–10	0.191	1.27	0.076
Total sequence	>10	0.222	1.34	10^{-5}

The parameters are solved for an M 6.04 mainshock and aftershocks $M \geq 4.8$. The first row gives parameters for direct aftershock sequences. The remaining rows give parameters for total aftershock sequences (made up of direct and secondary aftershocks). Total sequence parameters are given as a single parameter set that averages over all times and as separated parameter sets that give more accurate solutions for shorter time periods.

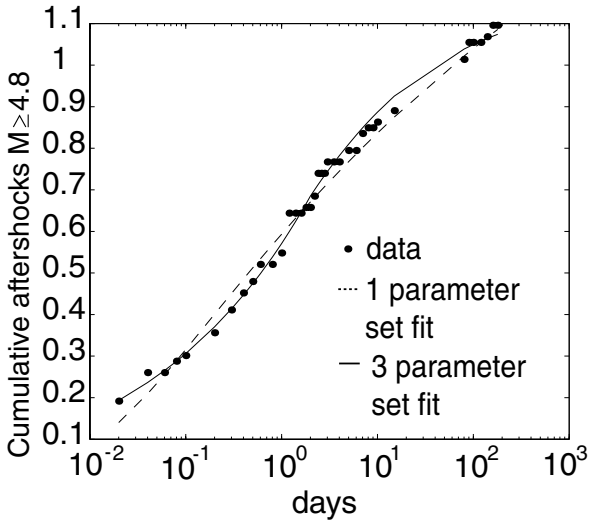

Figure 3. Cumulative number of $M \geq 4.8$ aftershocks recorded in the average aftershock sequence of an M 6.04 California mainshock, as calculated from the aftershock sequences of 73 $M \geq 5$ California mainshocks that occurred between 1976 and 2000. The data are fit with a single modified Omori law (dashed line) and a modified Omori law that undergoes parameter changes at days 2 and 10 (solid line). The change in Omori parameters with time is caused by the presence of secondary aftershocks. Parameters are given in Table 3.

by Reasenberg and Jones (1989) (0.1163 versus 0.2873). The A_T parameter solved for by Reasenberg and Jones (1989) is now known to have been biased upward by about a factor of 2 because they solved for parameters from individual aftershock sequences instead of a stack and thus only used the more active sequences, for which parameters could be solved for most robustly (L. M. Jones, personal comm., 2002).

Using the best-fit direct and total parameters and equation (4), we solve for the fraction of cumulative aftershocks that are secondary. We obtain reasonable agreement between these results and the predictions made by Monte Carlo trials with our synthetic aftershock model (Fig. 4A). Our agreement with the simulation results deteriorates, however, when we use the same parameters to predict what fraction of ongoing aftershocks should be secondary (equation 2; Fig. 4B). This is because equation (2) is particularly sensitive to the temporal changes of the total Omori parameters.

To answer this difficulty we approximate the smooth change in total sequence Omori parameters by fitting the total sequence with three different sets of modified Omori parameters, with the changeover between parameter sets occurring at days 2 and 10 of the sequence. These changeover days give the best least-squares fit to the data (Fig. 3). We find that the least-squares error between the modified Omori law function and the data decreases by 14% when we use two parameter sets rather than one and decreases by 57% when we use three parameter sets rather than one. An alternative mathematical solution to breaking the sequence into three parts is derived by Helmstetter and Sornette (2002).

Even with the three sets of parameters the predictions of equation (2) and the simulation results agree poorly for durations less than about 0.3 days. This is because the *c*-value, which is important at short times, is quite different for the two sequences, with $c_D = 0.085$ days and $c_T = 10^{-5}$ days. This value for c_T holds even if we only look at the first few data points in the sequence. The problem may be intrinsic with the *c* parameter itself. The parameter is used to correct for the fact that the power law becomes infinite as *t* goes to zero; but is not really a true fix since the modified Omori law with a nonzero *c* parameter has a nonzero aftershock rate even at $t = 0$. This implies that the mainshock and aftershock should happen at precisely the same moment, which, under laws of cause and effect, is clearly nonphysical. One potential solution is to introduce a Heaviside function such that there are simply no aftershocks before some time t_0 and a pure power law afterward (Kagan and Knopoff, 1981). The *c*-parameter problem should not be important over time periods longer than about half a day.

In general our results indicate that the fraction of aftershocks that are secondary after an *M* 6.04 mainshock is not insignificant, especially for ongoing aftershocks occurring at least several days after the mainshock. For additional insight into the solution we also plot separate time series of the direct, secondary, and total aftershock rates (Fig. 5).

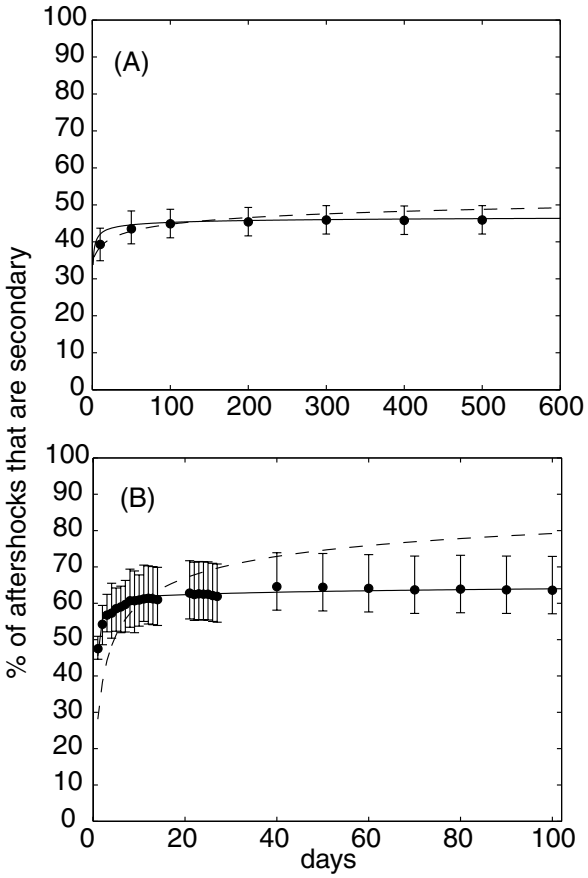

Figure 4. (A) The percentage of cumulative aftershocks of an average *M* 6.04 California mainshock that should be secondary, as a function of time, as calculated from equation (4) using the single best-fit modified Omori law parameter set (dashed line) and best-fit triple set of total sequence modified Omori law parameters (solid line). Both fits produce similar results. (B) The percentage of ongoing aftershocks of an average *M* 6.04 California mainshock that should be secondary as a function of time, as calculated by equation (2) using the best-fit modified Omori law single parameter set (dashed line) and the best-fit modified Omori law triple parameter set (solid line). In this case, the two solutions diverge by nearly 20% after 100 days. The calculation using the triple parameter set is much closer to results from model simulations (black dots). Each model data point represents the average of 1000 Monte Carlo trials. Error bars on the black dots indicate the 95% range of values observed with the Monte Carlo trials.

Variation of the Fraction of Aftershocks that are Secondary with Mainshock Magnitude

In all of our secondary aftershock calculations we are concerned only with aftershock sequences in which no aftershock is larger than the initial mainshock. This restriction is made because if an aftershock larger than the mainshock occurs, it is obvious that most aftershocks will be secondary. Using this restriction, however, causes secondary aftershock production to vary with mainshock magnitude.

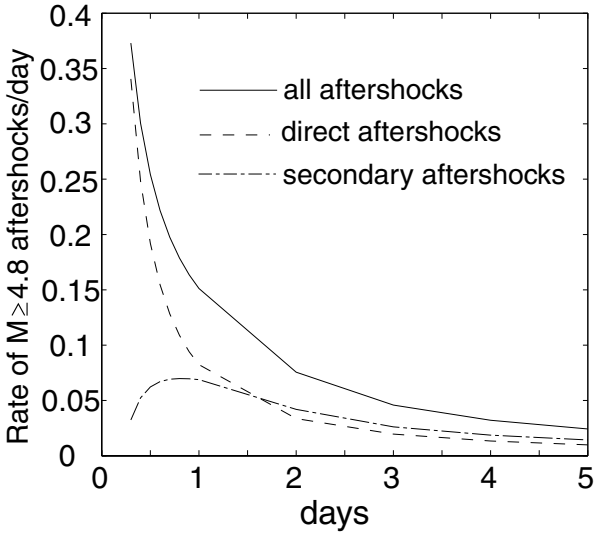

Figure 5. Direct, secondary, and total aftershock rates for the average M 6.04 California mainshock, calculated using equation (2) and the best-fit triple set of modified Omori parameters. Initially the vast majority of aftershocks are direct; but the direct aftershock rate decays quickly and is overtaken by the secondary aftershock rate within 2 days. The graph is started at 0.3 days since we find that equation (2) cannot be used accurately for earlier times.

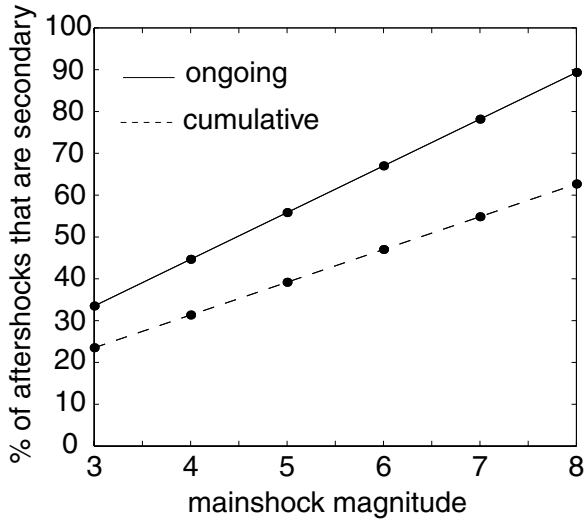

Figure 6. The average percentage of cumulative and ongoing aftershocks that are secondary as a function of mainshock magnitude, after 10 years, for California aftershock sequences in which no aftershock is larger than the mainshock.

As noted earlier, each unit magnitude range of earthquakes contributes equally to aftershock production, so each magnitude unit of direct aftershocks is expected to generate equal fractions of the secondary aftershock population. Thus if we eliminate all aftershocks larger than the mainshock, and their progeny, we will eliminate few direct aftershocks, but the fraction of secondary aftershocks eliminated will be equal to the fraction of magnitude ranges eliminated. That is, the fraction of total aftershocks that are secondary will be proportional to the number of magnitude units that are smaller than the mainshock. Therefore if we have a minimum magnitude $M_{\min}$ and a mainshock magnitude M, the average fraction of aftershocks that are secondary if we only consider sequences in which all aftershocks are smaller than M is given by

$$S(M) = \frac{M - M_{\min}}{6.04 - M_{\min}} \times S(6.04), \qquad (6)$$

where $S(M)$ is the fraction of aftershocks that are secondary after a mainshock of magnitude M and $S(6.04)$ is the average fraction of earthquakes that are secondary in the aftershock sequence of an M 6.04 mainshock, which we have already calculated. (Any other reference mainshock magnitude may also be used for which the fraction of secondary aftershocks is known.) Using this equation with $M_{\min}$ set to 0, we solve for the average fraction of aftershocks that are secondary for average California sequences 10 years after the mainshock as a function of mainshock magnitude. We find that over 50% of aftershocks produced after the eighth day of the sequence are secondary for $M \geq 5$ mainshocks and over 50% of all aftershocks are secondary for $M \geq 7.0$ mainshocks that have aftershock sequences lasting for at least 15 days (Fig. 6).

Predicting Aftershock Locations

We have shown that many aftershocks are secondary, especially following large mainshocks. It does not automatically follow, however, that the common practice of calculating only mainshock-induced stress changes to predict future aftershock locations (e.g., Papadimitriou and Sykes, 2001) could be significantly improved by including aftershock-induced stress changes. This is because the aftershocks might primarily reinforce, rather than modify, the mainshock-induced stress change pattern.

One way to determine whether including aftershock-induced stress changes is important would be to model stress changes produced by a mainshock and its suite of aftershocks and then see if the areas of stress increase changed significantly as the sequence progresses. It would be extremely difficult to do such a calculation, however, because many aftershocks are missing from catalogs, especially near the beginning of sequences; focal mechanisms are often uncertain and the correct fault plane difficult or impossible to select; and aftershock rupture inversions may be quite difficult to calculate. Alternatively, we might carry out the calculation with synthetic mainshock and aftershocks, but such a model would also be extremely difficult to build. There are too many modeling unknowns, one of the most important

being how to set up a realistic fault network with numerous small faults that is kinematically stable.

It is possible to approach the problem from a different angle. Namely, if we can demonstrate that a prediction scheme, any prediction scheme, that neglects mainshock-induced stress change and uses only information from previous aftershocks performs significantly better than a standard prediction scheme using only mainshock-induced stress changes, then it is clear that the presence of secondary aftershocks is of practical importance for the purpose of forecasting. Or at least it is clear that the tendency of aftershocks to cluster with each other in time and space gives quite useful forecasting information.

Toward this end we compare the predictive abilities of mainshock-induced static Coulomb stress change calculations and a time-updated method of our own design, called the probability map method, that uses no information about the mainshock but calculates the probability of new aftershocks occurring in different locations based on the timing, location, and magnitudes of previous aftershocks. These two methods do not, of course, exhaust the possibilities of what we could compare. For the stress change induced directly by the mainshock, we could also, for example, use dynamic stress (e.g., Kilb, 2003), viscoelastic stress (e.g., Zeng, 2001; Freed and Lin, 2002) or pore pressure change (e.g., Bosl and Nur, 1997). We chose static Coulomb stress change because it is commonly used and easy to calculate. In addition, static stress changes can often be used as an estimate for dynamic and viscoelastic stress changes. Alternative schemes for predicting aftershock locations based on previous aftershock parameters include methods proposed by Wiemer (2000) and Jackson and Kagan (1999). Both of these methods are more complex and refined than our probability maps and require a number of additional calculations. In addition, the method of Wiemer (2000) is based on the idea that the Gutenberg–Richter *b*-value and modified Omori *p*-value vary spatially over the aftershock zone, which is not a universally accepted concept; the idea of *b*-value variation in particular runs counter to the findings of Woo (1997). So for simplicity we do not include the Wiemer (2000) and Jackson and Kagan (1999) methods at this time.

The results of our comparison will be specific to our study area of California since the quality of aftershock catalog and mainshock slip inversion data varies from place to place. We do our comparison for the North Palm Springs, Joshua Tree, Landers, and Hector Mine sequences, for which we have gridded static Coulomb stress change data from Stein *et al.* (2003). For all of the aftershock sequences we use the aftershock zone boundaries given in Table 1 and consider as aftershocks all earthquakes occuring within these boundaries through the end of December 2001, except for Joshua Tree aftershocks, which can no longer be independently identified and are thus truncated at the time of the Landers mainshock, and Landers aftershocks, which are similarly truncated at the time of the Hector Mine mainshock.

The Coulomb stress change calculations from Stein *et al.* (2002) are done at 7 km depth and resolved onto vertical, optimally oriented strike-slip fault planes, which are calculated using regional N7°E maximum compression.

Aftershock Probability Maps

The probability map method is based on the premise that the location of future aftershocks is significantly influenced by the timing, concentration, and magnitude of previous aftershocks. The method uses no information about the fault or slip parameters of the mainshock. We find that the probability map method works best for sequences with at least 50 recorded aftershocks.

The essence of the probability map method is that each point in the aftershock zone is assigned to one of several predefined regions based on the point's proximity in time and space to previous aftershocks. The specific probability of a particular point hosting a future aftershock is then determined based on the percentage of the preceding group of N aftershocks that located in the same region. This purely empirical method of solving for probabilities is not common with other techniques (e.g., Jackson and Kagan, 1999; Wiemer, 2000) but has the significant advantage that unknown factors such as unrecorded aftershocks and the degree of location and magnitude assignment error are taken into account automatically as long as the new set of aftershocks is affected by these factors to a similar degree as the preceding N set of aftershocks was.

To define the different aftershock regions we first draw square influence zones around each aftershock epicenter, as described earlier. Region 1 is defined as the map area that is not contained within any influence zone. The other regions are within the influence zones and are based on the timing and concentration of previous aftershocks. We take into account whether an influence zone is older or younger than a cutoff age t (where the age of an influence zone is defined as the time elapsed since the aftershock that created it) and whether the number of influence zones overlapping at a particular point are above or below a cutoff number L. This gives us four additional mutually distinct regions. In total the five regions cover the entire aftershock zone. A given point in the aftershock zone is in region 1 if it is not in any influence zone; region 2 if it is in 1 to $L - 1$ influence zones, all of which are more than t days old; region 3 if it is in 1 to $L - 1$ influence zones, at least one of which is less than t days old; region 4 if it is in L or more influence zones, all of which are more than t days old; and region 5 if it is inside of L or more influence zones, at least one of which is less than t days old.

We limit our number of regions to five in order to maintain statistical robustness in the empirical measurement of the probabilities. The boundaries of the regions will vary with time, and the regions are noncontiguous. As mentioned previously, at forecast time the probability of a new aftershock occurring in any region is set equal to the percentage of the preceding N aftershocks that occurred in the same region. It is important that N not be too large, because the

distribution of aftershocks between the different regions may change with time. By definition, for example, there are no aftershocks in regions 2 or 4 before time t has elapsed, so there is a significant readjustment after time t. In addition, after a large aftershock there is a sharp, transitory increase in the probability of aftershocks occurring in regions 3 or 5. N must be small enough, therefore, to capture these temporal changes, while at the same time be large enough to produce reliable statistics. Through trial and error we find that $N = 50$ is optimal for the nine sequences listed in Table 1. For smaller aftershock sequences smaller N values may be necessary, but we find that N values smaller than about 25 should not be used.

Similarily to N, the values of L and t must be chosen to strike a balance. If L is too large then the very densest clusters will be clearly highlighted, but the medium-size and smallest clusters will all be combined together in the same region, so the higher probability associated with the medium-size clusters will not be differentiated. Likewise, making L too small means the combination of large, medium, and small clusters in a single region, causing the larger probability associated with both the large and medium clusters to be missed. The choice of t is subject to similar constraints. Through trial and error with the nine aftershock sequences listed in Table 1, we find that the best balance can be achieved with $L = 5$ and $t = 0.5$ days. For individual sequences with fewer aftershocks than average, we find that even better results may be acheived with L set equal to 3 or 4. The best L and t values for a particular aftershock sequence cannot really be determined until the sequence is over, however, making the values irrelevant for forecasting purposes. Thus we feel that the most appropriate way to test the forecasting power of the probability maps against the Coulomb stress change maps is to use uniform, preset values of L and t for all of the sequences.

Once we define the regions and estimate the probability of each region containing aftershocks, we can make a probability map for the location of future aftershocks. This is done by first covering the entire aftershock zone with a dense grid. The smallest earthquake that we use to make our maps is M 2, which has an influence zone half-length of about 0.11 km, so we use a grid spacing of 0.1 km. The probability of the next aftershock occurring at each grid point is then set equal to the probability of an aftershock occurring in the region that the grid point is in, divided by the total number of grid points in that region. We choose M 2 as our magnitude cutoff for making the maps after finding that smaller earthquakes have such small influence zones in comparison to their location error that the very marginal information gained from using them is not worth the extra calculation time.

The grid points are so closely spaced that making individual forecasts for each grid point is practically meaningless given location error on the order of 2 km. Therefore we next cover the map with square cells with dimensions of 2.5 by 2.5 km. A summation is done over all of the grid points in each cell to get the total probability of the next aftershock occurring within it.

One disadvantage of our method is that since the regional boundaries change with the occurrence of each new aftershock, new forecasts have to be issued each time an aftershock occurs. In practice, it could be difficult to calculate aftershock parameters quickly enough to do this in real time, especially during the early, active part of an aftershock sequence. Thus we also make and test probability maps that are only updated at midnight and used to forecast the next 24 hr of activity. We refer to these as "24-hr probability maps" and to the maps that are continuosly updated as "real-time probability maps."

Evaluating the Aftershock Probability Maps and Coulomb Stress Change

We next compare how well the probability map and the static Coulomb stress change map methods predict aftershock locations. We use the Wilcoxon signed-rank test for correlated samples (Weiss and Hassett, 1982; Kilb and Rubin, 2002) to determine whether one method is significantly better than the other. To use this test, we first rank the cells on the probability and Coulomb stress change maps with a rank of 1 assigned to the cell with the highest assigned probability or the largest positive stress change, and so on. If two or more cells on a given map have the same probability or stress change we assign them the same rank, which is equal to the rank the lowest cell would have had if they were unequal. The rank of the cell that an aftershock occurs in then tells us how well the aftershock was predicted. If an aftershock occurs in the cell ranked 1 or 2, for example, then the prediction map did an excellent job at pinpointing the most likely aftershock location.

For each aftershock in our sample we record the rank of the cell that it occurred in on the probability map and on the static Coulomb stress change map. Our sample of aftershocks excludes the first 50 aftershocks of each sequence because these are needed to initialize the probability map, but it includes every other $M \geq 2.5$ aftershock of the North Palm Springs, Joshua Tree, and Hector Mine sequences and every other $M \geq 3.5$ aftershock of the considerably larger Landers sequence. A histogram of the static Coulomb stress change map ranks minus the real-time probability map ranks (Fig. 7) is made for each sequence. Note that more aftershocks on the right-hand side indicates that the probability map is performing better, and vice versa. It can be observed that all of the histograms contain more aftershocks on the right-hand side, and the Wilcoxon signed-rank test confirms with over 99.9% confidence that for each aftershock sequence the real-time probability map makes more precise predictions than the static Coulomb stress change map. That is, for each case the null hypothesis that differences in cell ranks are due to simple random fluctuations rather than systematic differences can be confidently rejected.

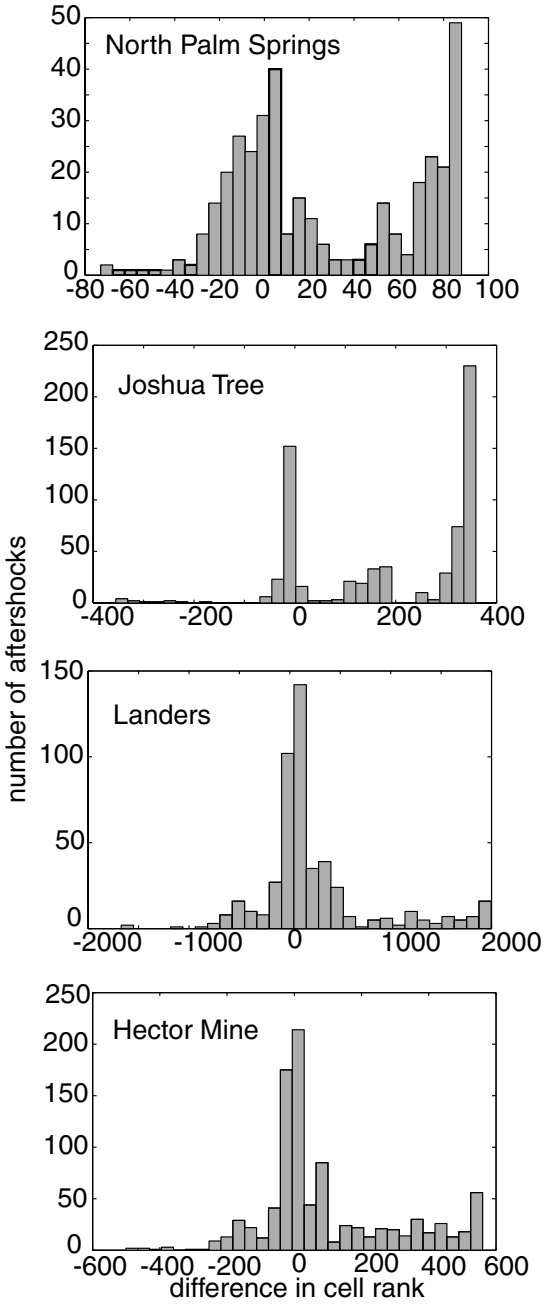

Figure 7. Comparing the aftershock location prediction precision of the static Coulomb stress change map and probability map. To do the comparison the cells on each map are ranked according to their predicted likelihood of containing an aftershock, with a rank of 1 corresponding to the highest probability. When an aftershock occurs, the rank of the cell that it occurred in on the probability map is subtracted from the rank of the same cell on the static Coulomb stress change map. A positive answer means that the probability map predicted the location of the aftershock more accurately, while a negative answer means that the Coulomb stress change map made the better prediction. The right-handed skewness of all of the histograms indicates that the probability map is performing better overall. Peaks on the right-hand side of the graphs for the North Palm Springs and Joshua Tree sequences indicate where large secondary aftershock clusters caused concentrated deviations from the Coulomb stress change predictions.

We also use the Wilcoxon signed-rank test to compare the predictive ability of the Coulomb stress change map with the 24-hr updated probability map. The contrast between the predictive ability of these two maps is on the order of 25% smaller, but we can still say with over 99.9% confidence that the 24-hr probability map predicts more precisely than the static Coulomb stress change map for each of the sequences.

An additional way to compare the two prediction methods is to plot the total number of cells that need to be identified by each method in order to forecast the locations of a given percentage of the aftershocks. As an example, consider an aftershock zone that is covered by 100 cells. At each forecast time we want to identify a set of cells such that 50% of all of the aftershocks in our forecast interval will occur within some cell that we have identified, but such that the number of extraneous cells included in our set is kept to a minimum. The smaller the number of cells that we can identify and still capture 50% of the seismicity, the better our forecasting method is performing.

The number of cells that are needed to locate different percentages of the aftershocks with the different methods (static Coulomb stress change map, real-time probability map, and 24-hr probability map) are given in Figure 8. For reference, each figure also contains a line that indicates the best prediction that could have been made and a line that indicates the average prediction that would have resulted from random guessing. The best-prediction-possible line is calculated from the completed aftershock sequence by retrospectively ranking each cell according to the number of foreshocks it ended up containing. The random-guess line and corresponding 95% confidence intervals are calculated from 1000 Monte Carlo trials.

Figure 8 indicates that in general both the static Coulomb stress change maps and probability maps provide predictions significantly better than random guessing, and the general ability of both methods to identify the most densely populated cells, where about 20%–40% of the aftershocks will occur, is comparable. The probability maps, however, are uniformly better than the Coulomb stress change maps at selecting the cells in which most of the remaining aftershocks will occur. The only exception is the most scattered 1%–10% of the aftershocks, which neither method shows any significant ability to anticipate (Fig. 8). We also note that the shapes of the probability map forecast curves in Figures 8 and 13 are quite similar to curves that describe how well the spatial distribution of the small earthquakes in a catalog measured over a limited time period can predict the locations of large earthquakes for years afterward (Kafka and Levin, 2000; Kafka, 2002).

One surprising result is that while the static Coulomb stress change map performs better than random guessing for nearly all of the aftershocks in the Landers and Hector Mine sequences, for some of the Joshua Tree and North Palm Springs aftershocks the static Coulomb stress change map actually performs worse than random guessing (Fig. 8, left-hand side). This is probably due to the near-fault presence

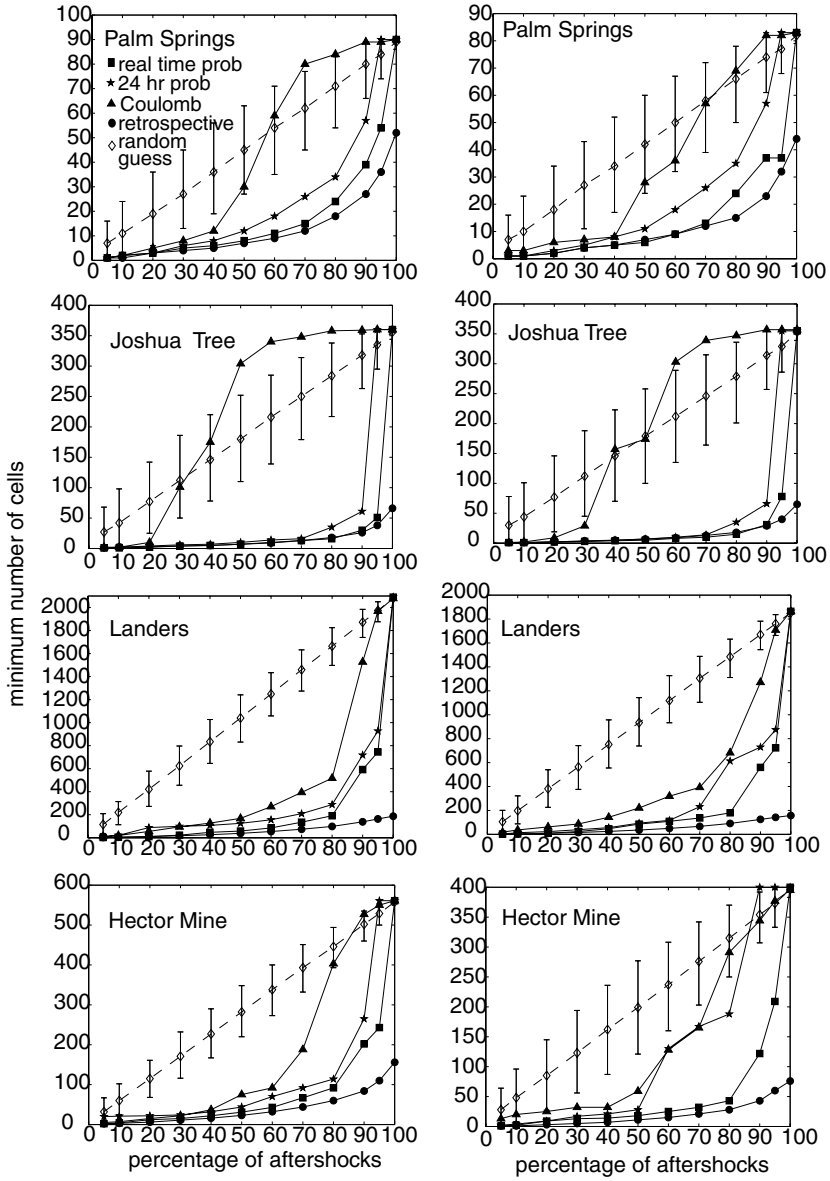

Figure 8. Comparison of aftershock location forecasts made by the probability maps and by Coulomb stress change calculations. On the left are calculations done for the entire aftershock sequence; on the right are calculations done for only those aftershocks located away from the main fault plane. For the Joshua Tree, Landers, and Hector Mine earthquakes this is done by eliminating all cells experiencing more than an absolute value of 8 bars of stress change from the mainshock; for the smaller North Palm Springs earthquake we eliminate all cells experiencing more than 5 bars of stress change. The percentage of aftershocks are plotted versus the number of (2.5 by 2.5 km) cells that need to be identified by each forecasting method in order to have this percentage of aftershocks contained. Squares give results for the real-time probability map forecasts, stars for the 24-hr probability map forecasts, and triangles for the Coulomb stress change calculations. For reference, the filled circles give the best prediction that would have been possible, measured from the minimum number of cells needed to cover different percentages of aftershocks in the completed sequence, and the empty diamonds give the results that would be obtained if the likelihood of each cell having aftershocks were guessed randomly. The random-guess results and accompanying 95% confidence intervals are calculated from 1000 Monte Carlo trials with each aftershock sequence. For each sequence, the overall best forecasting is provided by the real-time probability maps, with the next best forecasts provided by the 24-hr probability maps.

of some cells with highly negative static Coulomb stress changes. These cells will be ranked as the least likely to contain aftershocks, but since they are in the near-fault region they may contain many secondary aftershocks. The assignments of negative stress change to these cells may also be in error due to inaccuracies in determining the mainshock slip distribution; calculated near-fault stress changes are extremely sensitive to the slip distribution and background stress orientation used (e.g., Kilb *et al.*, 1997). Thus we make new graphs for only those aftershocks occurring in cells experiencing less than an absolute value of 8 bars of stress change for the Joshua Tree, Landers, and Hector Mine earthquakes and less than 5 bars of stress change for the North Palm Springs mainshock (Fig. 8; right-hand side). This eliminates most of the near-fault aftershocks of each mainshock. Toda *et al.* (1998) similarily used an 8-bar cutoff to eliminate near-fault aftershocks of the 1995 Kobe earthquake. We find that the Coulomb map predictions indeed improve when the near-fault area is eliminated, but remain worse than the real-time and 24-hr probability map predictions (Fig. 8), with the exception of the 24-hr prediction for the Hector Mine aftershocks, for which the two predictions appear comparable. This may be because an unusually large proportion (2/3) of aftershocks in the Hector Mine sequence occured in near-fault cells and were eliminated. We also investigate whether the relative predictive ability of the static Coulomb stress change and probability maps varies with aftershock location and aftershock magnitude. We find that location is important; even with the near-fault stress change calculation errors, the static Coulomb stress change map has a definite advantage in the near-fault region (Fig. 9). This is not surprising since the mainshock fault location is a primary input to the Coulomb stress change calculation, while it is neglected in the probability map calculation.

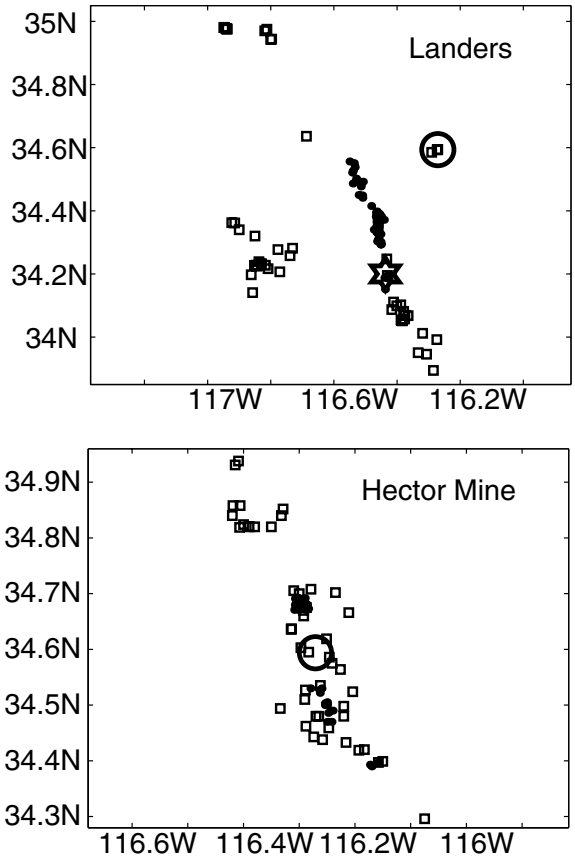

Figure 9. Black dots indicate the 50 aftershocks of the Landers and Hector Mine earthquakes best predicted by the Coulomb stress change calculations; open squares indicate the 50 aftershocks best predicted by the probability map calculations. There is some overlap between the two data sets, but, as expected, the Coulomb stress change is better at predicting aftershocks lying near the mainshock fault plane (presumably direct aftershocks) while the probability map is better at predicting the more distributed, (and presumably secondary), aftershocks. The epicenters of the Landers and Hector Mine earthquakes are denoted by a large star and circle, respectively.

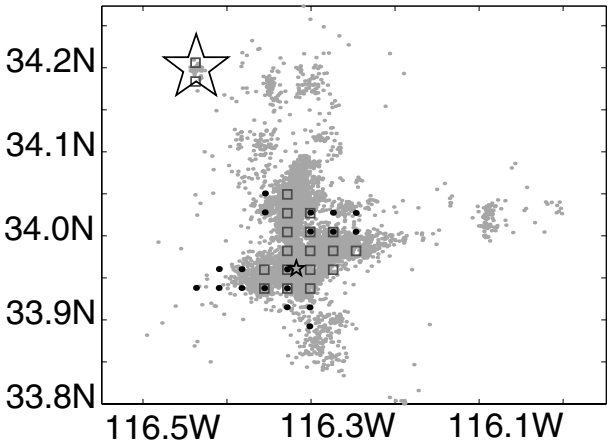

Figure 10. Comparison of the 5% of cells identified to be the most likely to contain the next Joshua Tree aftershock by the mainshock-induced static Coulomb stress change calculation (black dots) and probability map method (gray squares) right before the Landers earthquake occurred. (Note that some of the circles and squares overlap.) Small and large stars denote the epicenters of the Joshua Tree and Landers earthquakes, respectively.

The relative ability of the two methods to predict an aftershock does not vary with aftershock magnitude at the 95% confidence level. Just as the probability map method predicts aftershock locations more precisely than the static Coulomb stress change map in general, it also more precisely predicts the locations of the largest aftershocks. Specifically, it is interesting to note that the real-time probability maps do a much better job than the Coulomb stress change map at pinpointing the locations of the Landers (Fig. 10) and Hector Mine epicenters, primarily a result of the fact that both of these earthquakes nucleated at some distance from their respective mainshock faults (hence low Coulomb stress change) but had active foreshock sequences (hence the strong identification by the probability map method.) We note that the actual static stress change at the Hector Mine epicenter does remain controversial (Harris and Simpson, 2002). Specific comparisons of the two methods for all $M \geq 5$ aftershocks are given in Table 2.

One caveat for our results is that we may not have used the best method to rank cells on the static Coulomb stress change map. We rank the cells simply according to the amount of positive Coulomb static stress change they experience, which is in keeping with how static Coulomb stress change is often applied to predict aftershock locations. When Coulomb stress change is applied in conjunction with rate and state friction theory, however, a stress step changes the rate of ongoing seismicity by a given multiple, so the probability of having an aftershock in a given cell actually becomes a combined function of the stress change and the preexisting seismicity rate. Yet we note that static Coulomb stress change studies that incorporate the effect of preexisting seismicity rates do not appear to show any large predictive improvement over studies that use static Coulomb stress changes by themselves (compare Hardebeck *et al.* [1998] and Toda *et al.* [1998]). So we feel justified for now in simply ranking the cells according to the amount of positive static Coulomb stress change they experience, with the idea that this might be refined in future studies.

In addition to the better performance we find here, there are also other benefits to be gained from using a probability-map-type method for aftershock prediction rather than, or in addition to, static Coulomb stress change maps. For one, the probability map method is potentially faster; it can be used as soon as 50 aftershocks have been located—there is no need to wait for a mainshock slip inversion. For another, the probability maps not only identify which cells are most likely to contain an aftershock but also assign a specific aftershock probability to each cell. We evaluate how well these

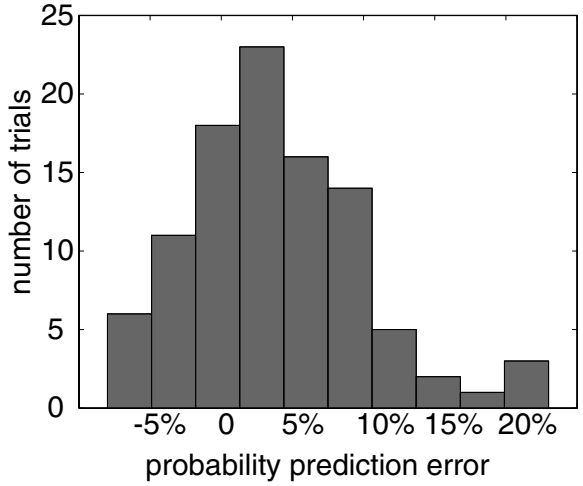

Figure 11. Error distribution of how well the probability maps predict the actual probability that a given set of cells will contain the next aftershock. For each aftershock sequence in Table 1 we measure what percentage of aftershocks occurs in the sets of probability map cells that add up to 5%, 10%, 20%, 30%, 40%, 50%, 60%, 70%, 80%, 90%, and 95% of the total probability. The sets are specifically chosen such that the target probability is obtained with the smallest possible total number of cells. The histogram gives the differences between the measured percentages and predicted probabilities. The distribution is skewed to the right, meaning that the cells assigned the highest probability of having an aftershock actually contain slightly more aftershocks than expected and cells assigned the lowest probabilities have somewhat fewer aftershocks than expected. For nearly 90% of the trials the difference between the predicted probability and percentage of aftershocks measured is less than 10%.

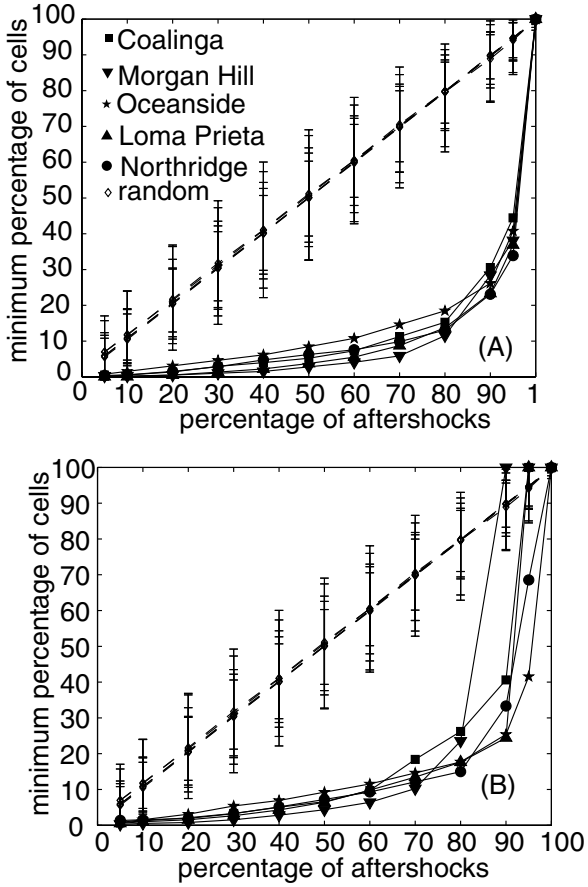

Figure 12. Results of using the probability map to forecast the aftershocks of the Coalinga, Morgan Hill, Oceanside, Loma Prieta, and Northridge earthquakes. The percentage of aftershocks is plotted against the percentage of the cells covering each aftershock zone that need to be identified by the probability map method in order to forecast them. Results are given for (A) real-time probability map forecasts and (B) 24-hr probability map forecasts. Forecasts for all five of the aftershock sequences show similar success rates, suggesting that the probability map method provides forecasts of a consistent quality.

specific probabilities are estimated by measuring what percentage of the aftershocks occur in the sets of cells that add up to 5%, 10%, 20%, 30%, 40%, 50%, 60%, 70%, 80%, 90%, and 95% of the total predicted probability. The sets of cells are chosen such that each set contains as few cells as possible. We calculate the differences between the predicted probabilities and the actual aftershock percentages (Fig. 11). We find that the error distribution is skewed to the right, meaning that the cells with the highest probabilities tend to contain a slightly larger percentage of aftershocks than predicted, and vice versa. Overall nearly 90% of the probability map probability forecasts are correct to within 10%. We also find that the probability map method produces predictions that are consistent in quality for different aftershock sequences (Fig. 12).

Finally it is important to note that both the Coulomb stress change calculations and the probability map method provide information only on the most likely location of aftershock epicenters. They provide no information about how many aftershocks are likely to occur, about the magnitude of those aftershocks, or about the extent of area that may be affected by the aftershocks. Estimates of these properties can best be made by combining a local Omori's law with secondary activity accounted for with the Gutenberg–Richter relationship and ground-motion calculations. An example of such a forecasting method is given by Gerstenberger *et al.* (2001).

Conclusions

We find that many triggered earthquakes are actually secondary aftershocks—aftershocks of previous aftershocks—and are thus not constrained to occur where the mainshock increased stress. The percentage of aftershocks in a sequence that are secondary increases with time and mainshock magnitude. For the average California aftershock

sequence of an M 6 mainshock with no aftershocks larger than the mainshock, we find that over 35% of all aftershocks and over 50% of ongoing aftershocks are secondary 10 days after the mainshock. For the average M 7 mainshock over 40% of the total and nearly 70% of ongoing aftershocks are secondary over the same time period.

Because secondary aftershocks are common we should expect many aftershocks to occur near previous, recent aftershocks. We find that a simple method for forecasting the distributions of aftershock epicenters based solely on previous aftershock locations, times, and magnitudes predicts aftershocks better than static Coulomb stress change calculations. We conclude that the effect of aftershock-induced stresses on the locations of future triggered earthquakes is significant.

Acknowledgments

We are very grateful to Ross Stein and coauthors for providing us with their unpublished static Coulomb stress change calculations. We thank Thorsten Becker and James Rice for close readings and comments that greatly improved this article. Debi Kilb, Paul Reasenberg, and associate editor Jeanne Hardebeck provided thorough, thoughtful, and timely reviews that significantly improved the text. We would also like to thank James Sethna, Nadia Lapusta, Emily Brodsky, Alan Kafka, John Ebel, Patricia Moreno, Debi Kilb, Mike Antolik, and Agnes Helmstetter for discussions and Yu Gu for discussions and invaluable technical assistance. Earthquake catalog data were made available by the Council of the National Seismic System, the Southern California Earthquake Data Center, the California Institute of Technology, the Northern California Earthquake Data Center, the Berkeley Seismological Laboratory, and the Northern California Seismic Network. K.R.F. was supported by an NSF graduate student fellowship for part of this work. Additional support was provided by the Southern California Earthquake Center. SCEC is funded by NSF Cooperative Agreement EAR-8920136 and USGS Cooperative Agreements 14-08-0001-A0899 and 1434-HQ-97AG01718. The SCEC contribution number for this article is 701.

References

Abercrombie, R. E. (1995). Earthquake and source scaling relationships, from -1 to 5 M_L using seismograms recorded at 2.5 km depth, *J. Geophys. Res.* **100,** 24,015–24,036.

Bender, B. (1983). Maximum likelihood estimation of b values for magnitude grouped data, *Bull. Seism. Soc. Am.* **73,** no. 3, 831–851.

Bosl, W. J., and A. Nur (1997). Numerical simulation of postseismic vertical displacement due to pore pressure changes following the 28 June 1992 Landers earthquake, *EOS* **78** (Fall Meet. Suppl.), 491.

Cao, T., M. D. Petersen, and M. S. Reichle (1996). Seismic hazard estimation from background seismicity in Southern California, *Bull. Seism. Soc. Am.* **86,** no. 5, 1372–1381.

Console, R., and M. Murru (2001). A simple and testable model for earthquake clustering, *J. Geophys. Res.* **106,** 8699–8711.

Das, S., and C. H. Scholz (1981). Off-fault aftershocks caused by shear stress increase? *Bull. Seism. Soc. Am.* **71,** no. 5, 1669–1675.

Dieterich, J. A. (1994). Constitutive law for the rate of earthquake production and its application to earthquake clustering, *J. Geophys. Res.* **99,** 2601–2618.

Felzer, K. R., T. W. Becker, R. E. Abercrombie, G. Ekström, and J. R. Rice (2002). Triggering of the 1999 M_W 7.1 Hector Mine earthquake by aftershocks of the 1992 M_W 7.3 Landers earthquake, *J. Geophys. Res.* **107,** no. B9, 2190, doi 10.1029/2001JB000911.

Freed, A. M., and J. Lin (2002). Accelerated stress buildup on the southern San Andreas Fault and surrounding regions caused by Mojave Desert earthquakes, *Geology* **30,** 3007–3010.

Gerstenberger, M. C., S. Wiemer, L. M. Jones, and D. Giardini (2001). Testing and implementation off real time probabilistic aftershock hazard mapping (abstract), *EOS* **82** no. 47 (Fall Meet. Suppl.), S41C-06.

Gomberg, J. (2001). The failure of earthquake failure models, *J. Geophys. Res.* **106,** 16,253–16,263.

Gross, S. J., and C. Kisslinger (1994). Test of models of the aftershock rate decay, *Bull. Seism. Soc. Am.* **84,** no. 5, 1571–1579.

Guo, Z., and Y. Ogata (1997). Statistical relationships between the parameters of aftershocks in time, space, and magnitude, *J. Geophys. Res.* **102,** 2857–2873.

Gutenberg, B., and C. F. Richter (1944). Frequency of earthquakes in California, *Bull Seism. Soc. Am.* **34,** no. 4, 185–188.

Hardebeck, J. L., J. J. Nazareth, and E. Hauksson (1998). The static stress change triggering model: constraints from two Southern California aftershock sequences, *J. Geophys. Res.* **103,** 24,427–24,437.

Harris, R. A., and R. W. Simpson (1992). Changes in static stress on Southern California faults after the 1992 Landers earthquake, *Nature* **360,** 251–254.

Harris, R. A., and R. W. Simpson (2002). The 1999 M_W 7.1 Hector Mine, California, earthquake: a test of the stress shadow hypothesis? *Bull. Seism. Soc. Am.* **92,** no. 4, 1497–1512.

Helmstetter, A., and D. Sornette (2002). Sub-critical and super-critical regimes in epidemic models of earthquake aftershocks, *J. Geophys. Res.* **107,** no. B10, 2237, doi 10.1029/2001JB001580.

Ishimoto, M., and K. Iida (1939). Observations of earthquakes registered with the microseismograph constructed recently, *Bull. Earthquake Res. Inst. Tokyo Univ.* **17,** 443–478.

Jackson, D. D., and Y. Y. Kagan (1999). Testable earthquake forecasts for 1999, *Seism. Res. Lett.* **70,** 393–403.

Kafka, A. L. (2002). Statistical analysis of the hypothesis that seismicity delineates areas where future large earthquakes are likely to occur in the Central and Eastern United States, *Seism. Res. Lett.* **73,** 990–1001.

Kafka, A. L., and S. Z. Levin (2000). Does the spatial distribution of smaller earthquakes delineate areas where larger earthquakes are likely to occur? *Bull. Seism. Soc. Am.* **90,** no. 3, 724–738.

Kagan, Y. Y. (1991). Likelihood analysis of earthquake catalogs, *Geophys. J. Int.* **106,** 135–148.

Kagan, Y. Y., and D. D. Jackson (1991). Long-term earthquake clustering, *Geophys. J. Int.* **104,** 117–133.

Kagan, Y. Y., and D. D. Jackson (2000). Probabalistic forecasting of earthquakes, *Geophys. J. Int.* **143,** 438–453.

Kagan, Y. Y., and L. Knopoff (1981). Stochastic synthesis of earthquake catalogs, *J. Geophys. Res.* **86,** 2853–2862.

Kanamori, H. (1977). The energy release in great earthquakes, *J. Geophys. Res.* **82,** 2981–2987.

Kanamori, H., and D. L. Anderson (1975). Theoretical basis of some empirical relations in seismology, *Bull. Seism. Soc. Am.* **65,** no. 5, 1073–1095.

Kilb, D. (2003). A strong correlation between induced peak dynamic Coulomb stress change from the 1992 M 7.3 Landers earthquake and the hypocenter of the 1999 M 7.1 Hector Mine earthquake, *J. Geophys. Res.* **108,** B1 2012, doi 10.1029/2001JB000678.

Kilb, D., and A. M. Rubin (2002). Implications of diverse fault orientations imaged in relocated aftershocks of the Mount Lewis, M_L 5.7, California, earthquake, *J. Geophys. Res.* **107,** no. B11, 2294, doi 10.1029/2001JB000149.

Kilb, D., M. Ellis, J. Gomberg, and S. Davis (1997). On the origin of diverse aftershock mechanisms following the 1989 Loma Prieta earthquake, *Geophys. J. Int.* **1997,** 557–570.

King, G. C., R. S. Stein, and J. Lin (1994). Static stress change and the triggering of earthquakes, *Bull. Seism. Soc. Am.* **84,** no. 3, 935–953.

Michael, A. J., and L. M. Jones (1998). Seismicity alert probabilities at Parkfield, California, revisited, *Bull. Seism. Soc. Am.* **88,** 117–130.

Mogi, K. (1962). On the time distribution of aftershocks accompanying the recent major earthquakes in and around Japan, *Bull. Earthquake Res. Inst. Tokyo Univ.* **40,** 107–124.

Ogata, Y. (1988). Statistical models for earthquake occurrence and residual analysis for point processes, *J. Am. Stat. Assoc.* **83,** 9–27.

Page, R. (1968). Aftershocks and microaftershocks of the Great Alaska Earthquake of 1964, *Bull. Seism. Soc. Am.* **58,** 1131–1168.

Papadimitriou, E. E., and L. R. Sykes. (2001). Evolution of the stress field in the northern Aegean Sea (Greece), *Geophys. J. Int.* **146,** 747–759.

Ranalli, G. (1969). A statistical study of aftershock sequences, *Ann. Geofis.* **22,** 359–397.

Reasenberg, P. A., and L. M. Jones (1989). Earthquake hazard after a mainshock in California, *Science* **243,** 1173–1176.

Richardson, E., and T. H. Jordan (2002). Seismicity in deep gold mines of South Africa: implications for tectonic earthquakes, *Bull. Seism. Soc. Am.* **92,** 1766–1794.

Richter, C. F. (1958). *Elementary Seismology*, W. H. Freeman, New York, 768 pp.

Rybicki, K. (1973). Analysis of afterhocks on the basis of dislocation theory, *Phys. Earth Planet. Interiors* **7,** 409–422.

Sornette, A., and D. Sornette (1999). Renormalization of earthquake aftershocks, *Geophys. Res. Lett.* **26,** 1981–1984.

Stein, R. S., and T. C. Hanks (1998). $M \geq 6$ earthquakes in Southern California during the twentieth century: no evidence for a seismicity or moment deficit, *Bull. Seism. Soc. Am.* **88,** 635–652.

Stein, R. S., A. A. Barka, and J. H. Dieterich (1997). Progressive failure on the North Anatolian Fault since 1939 by earthquake stress triggering, *Geophys. J. Int.* **128,** 594–604.

Stein, R. S., K. Richards-Dinger, S. Toda, S. Bozkurt, and T. Dewez (2003). Rate/state forecast animations of seismicity from earthquake stress changes in southern California, *G-cubed*, in preparation.

Taylor, M. A. J., R. Dmowska, and J. R. Rice (1998). Upper plate stressing and seismicity in the subduction earthquake cycle, *J. Geophys. Res.* **103,** 24,523–24,542.

Toda, S., R. S. Stein, P. A. Reasenberg, J. H. Dieterich, and A. Yoshida (1998). Stress transfer by the $M_W = 6.9$ Kobe, Japan earthquake: effect on aftershocks and future earthquake probabilities, *J. Geophys. Res.* **103,** 24,543–24,565.

Utsu, T. (1961). A statistical study on the occurrence of aftershocks, *Geophys. Mag.* **30,** 521–605.

Utsu, T. (1962). On the nature of three Alaskan aftershock sequences of 1957 and 1958, *Bull. Seism. Soc. Am.* **52,** no. 2, 279–297.

Weiss, N., and M. Hassett (1982). *Introductory Statistics*, Addison-Wesley, Reading, Massachusetts, 651 pp.

Wells, D. L., and K. J. Coppersmith (1994). New empirical relationships among magnitude, rupture length, rupture width, rupture area, and surface displacement, *Bull. Seism. Soc. Am.* **84,** 974–1002.

Wiemer, S. (2000). Introducing probabilistic aftershock hazard mapping, *Geophys. Res. Lett.* **27,** 3405–3408.

Wiemer, S., and M. Wyss (2002). Mapping spatial variability of the frequency-magnitude distribution of earthquakes, *Adv. Geophys.* **45,** 259–302.

Woo, G. (1996). Kernel estimation methods for seismic hazard source modeling, *Bull. Seism. Soc. Am.* **86,** no. 2, 353–362.

Yamanaka, Y., and K. Shimazaki (1990). Scaling relationships between the number of aftershocks and the size of the mainshock, *J. Phys. Earth* **38,** 305–324.

Zeng, Y. (2001). Viscoelastic stress-triggering of the 1999 Hector Mine earthquake by the 1992 Landers earthquake, *Geophys. Res. Lett.* **28,** 3007–3010.

Department of Earth and Planetary Sciences
Harvard University
20 Oxford St.
Cambridge, Massachusetts 02138
(K.R.F., G.E.)

Department of Earth Sciences
Boston University
685 Commonwealth Ave.
Boston, Massachusetts 02215
(R.E.A.)

Manuscript received 20 November 2002.